

# Long-Wavelength Avalanche Photodiodes Operating Over a 30 dB Optical Input Power Range

Alberto Ciarrocchi <sup>(1)</sup>, Wei Quan <sup>(1)</sup>, Maria Hämmerli <sup>(1)</sup>, Hektor Meier <sup>(1)</sup>

<sup>(1)</sup> Albis Optoelectronics AG, Moosstrasse 2A, 8803 Rüschlikon, Switzerland, [ac@albisopto.com](mailto:ac@albisopto.com)

**Abstract:** High-speed, long-wavelength, telecom and datacom 10 Gb/s and 25 Gb/s avalanche photodiodes (APDs) are sensitive to excessive optical input power. We explain this failure mechanism and demonstrate an optimized device structure reaching over +6 dBm optical damage threshold and verify it by testing in volume production. ©2022 The Author(s)

## Introduction

For over two decades, global network traffic has been growing exponentially. This trend is expected to continue, driven by data-intensive applications (AI, IoT, cloud etc...) and the mass adoption of faster networks, (fibre-to-the-home, 5G+ mobile services) [1, 2]. To accommodate the increasing demand, faster and more efficient photonic devices are needed. Avalanche photodiodes (APDs) are crucial to this effort, offering sensitivities that are several dB higher than those of PIN photodetectors thanks to their internal gain, drastically reducing the power budget for extended reach networks [3].

Despite being optimized for low-power optical signals ( $\sim 1 \mu\text{W}$  / -30 dBm), most practical applications of APDs require a very large dynamic range to ensure operation up to overload ( $\sim 500 \mu\text{W}$  / -3 dBm) and robustness to occasional fluctuations in optical input power up to a few mW [4]. However, most commercially available APDs are easily damaged when fed with excessive optical power [5], potentially causing expensive module replacement and extended downtimes. Furthermore, emerging APD applications such as OTDR or LiDAR require even higher tolerances, highlighting the

need for robust APDs.

Here we explain the optically-induced failure mechanism for mesa-type separated absorption, charge and multiplication (SACM) APD and present a new optimized mesa structure which extends the safe operation range for APDs up to and over +6 dBm optical input power. This improvement is demonstrated on 10 Gb/s (10G) and 25 Gb/s (25G) long wavelength APDs with low breakdown voltage and low noise.

## Optically-induced damage mechanism

During normal operating conditions, a strong electric field collects photogenerated primary carriers in the absorber layer. These drift into the multiplication region and undergo avalanche multiplication due to the high electric field, producing the internal gain of the device. Due to the sloped mesa sidewalls, the field is strong in the centre of the and low at the edge, thereby preventing carrier transport and avalanche multiplication close to the mesa surface (Fig. 1a).

However, for very high optical input power, the density of photogenerated primary electrons and holes can be high enough to screen the electric field in the absorber layer. This optical saturation

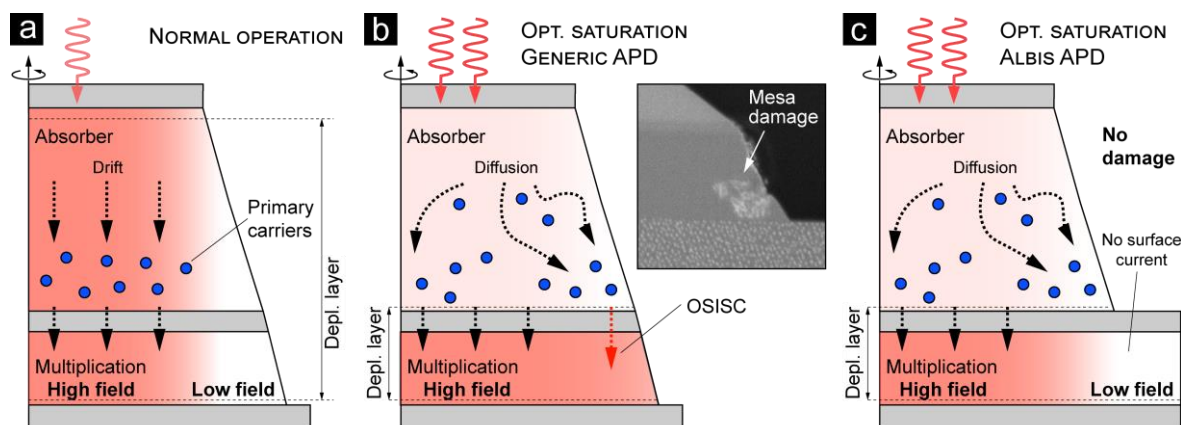


**Fig. 1:** Damage mechanism of APDs at high optical input power. (a) Normal operation of a generic mesa APD. (b) Generic APD under strong illumination. (c) Optimized mesa APD under strong illumination. The optimized structure confines the carriers to the centre of the multiplication layer under optical saturation. Darker red shading indicates higher electric field strength. Arrows indicate the flux of carriers: through the bulk (black) and along the surface (red). Thin dashed lines show the extent of the depletion layer. The images depict the cross section of half device, which has cylindrical symmetry.

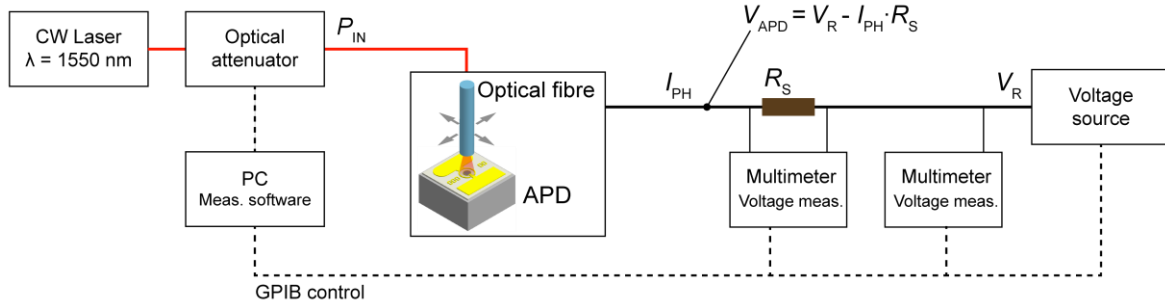


Fig. 2: Experimental setup.

regime is amplified by the APD voltage drop due to the large photocurrent flowing through the series resistance in presence of high optical input power. Another contribution comes from the heterojunction between the small-bandgap absorber and the larger-bandgap multiplication layer, typical in SACM APDs. This energy barrier inhibits the transport of primary carriers into the multiplication region at low electric fields, slowing down the evacuation of charges from the saturated absorber.

The reduction of the electric field in the absorber results in a transition from a drift-dominated to a diffusion-dominated carrier transport within the absorber layer. Under such conditions, primary carriers are free to diffuse towards the mesa sidewalls and enter the

multiplication region near the surface (Fig. 1b). Under optical saturation, the depletion layer retracts (dashed lines in Fig. 1b), making the electric field at the periphery of the multiplication layer stronger than under normal operating conditions. Therefore, the optical saturation-induced surface currents (OSISCs) along the mesa surface will undergo avalanche multiplication upon entering the multiplication layer, resulting in an extremely high surface current density. This causes local melting of the material and device failure as can be identified by SEM imaging of a focused ion beam cross-section of the damage site, as in the inset of Fig. 1b.

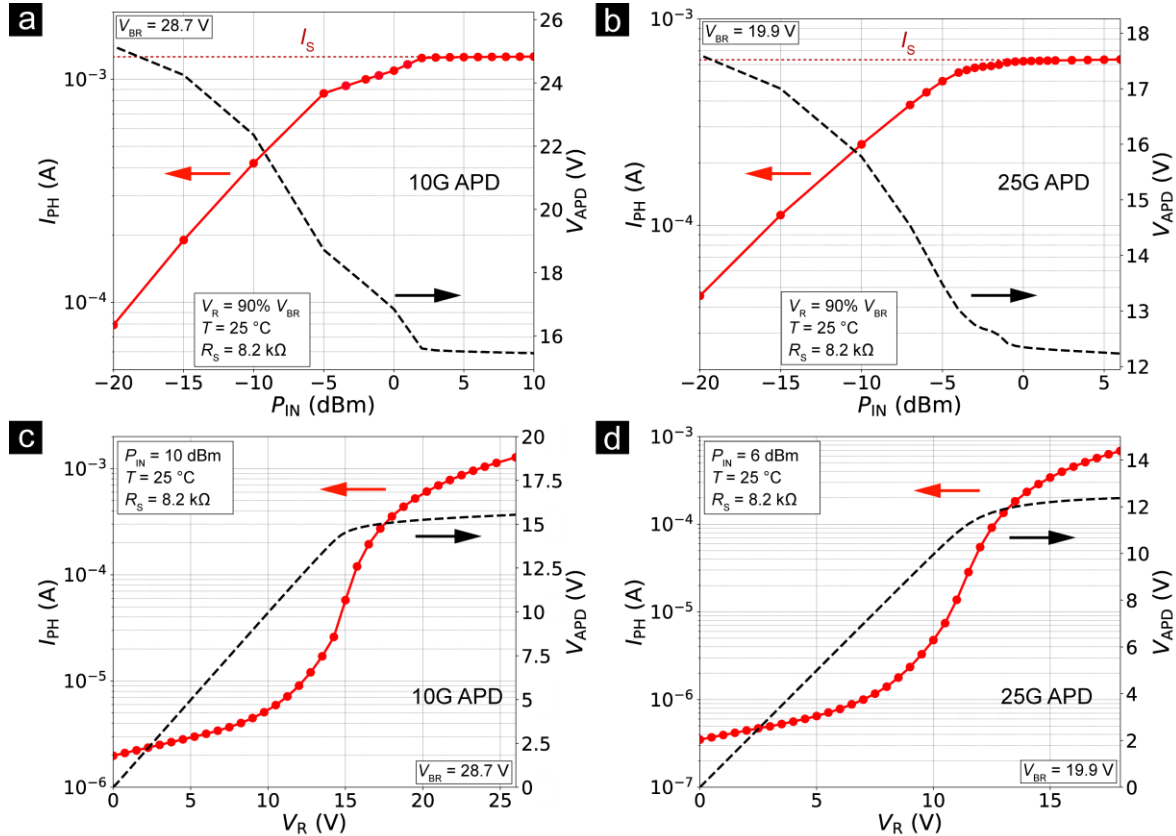


Fig. 3: Optical damage threshold testing for 10G APD and 25G APD. (a-b) Photocurrent  $I_{PH}$  and APD voltage  $V_{APD}$  vs. optical input power  $P_{IN}$  for  $V_R = 90\% V_{BR}$ . The dashed red line indicates the optical saturation current  $I_S$ . (c-d) Photocurrent  $I_{PH}$  and APD voltage  $V_{APD}$  vs. reverse bias voltage  $V_R$  for an optical input power  $P_{IN} = +6$  dBm (25G) or +10 dBm (10G).

### Optimized APD mesa structure

To overcome this issue, we fabricated SACM mesa-type APDs with an optimized structure. As shown in Fig. 1c, the effect of the optimized mesa is to confine the electric field in the multiplication layer to the centre of the device under optical saturation regime. We apply this concept to two different devices, a 10G APD and a 25G APD.

Sample APD chips were mounted on a chip carrier fixed to a motorized stage, in order to carefully align the active area to a SMF fibre. The test setup is shown in Fig. 2. The APDs were biased through a protective resistor  $R_S = 8.2 \text{ k}\Omega$ .  $R_S$  causes a reduction of the effective APD voltage ( $V_{APD}$ ) with respect to the applied bias  $V_R$ :

$$V_{APD} = V_R - R_S \cdot I_{PH}$$

The first test consists of ramping up the optical input power  $P_{IN}$  under a fixed reverse bias  $V_R = 90\% V_{BR}$ . As shown in Fig. 3a-b, for both devices the photocurrent  $I_{PH}$  increases with the applied optical input power. Above a certain value ( $P_{IN} \sim 0 \text{ dBm}$  for the 10G APD and  $\sim -2 \text{ dBm}$  for the 25G APD), the photo-response starts to flatten, since  $V_{APD}$  is close to the punch-through voltage, below which the APD turns off. In this regime  $V_{APD}$ , the electric field in the absorber and the generated photocurrent are balanced. We label the value of the photocurrent in this regime “optical saturation current” ( $I_s$ ), since any additional optical input power does not result in a higher photocurrent. The APD remains in this stable operating condition up to +6 dBm for the 25G APD and +10 dBm for the 10G device without any damage.

The second test is a sweep of the bias voltage  $V_R$  from 0 V to 90%  $V_{BR}$  under a fixed optical input power, simulating the device turning on in presence of strong optical signals.  $P_{IN} = +6 \text{ dBm}$  was used for the 25G APD and  $P_{IN} = +10 \text{ dBm}$  for the 10G APD. As shown in Fig. 3c-d, the photocurrent  $I_{PH}$  increases with the bias voltage  $V_R$ . No failures were detected, meaning that the optical damage threshold (ODT) is higher than +6

dBm and +10 dBm, for 25G and 10G APD respectively.

Based on this understanding of the optically-induced damage mechanism, a wafer-level screening procedure has been implemented at Albis Optoelectronics AG to test 100% of devices for their ODT prior to shipment [6].

### APD sensitivity and overload performance

The APDs were also tested for their frequency response, to ensure that the modifications did not affect their speed or noise performance. For this, APD ROSAs were realized by pairing the APDs with commercially available transimpedance amplifiers (TIAs). Fig. 4a-b show the sensitivity performance of the two builds. The device multiplied responsivity (at 90%  $V_{BR}$ , -20 dBm, 1550 nm) is 9.8 A/W for the 10G and 5.4 A/W for the 25G. The BER was determined by measuring the Q-factor with an Agilent 86100C oscilloscope.

For the 10G APD, the sensitivity is -31.2 dBm (BER = 1e-12) and -34.6 dBm (BER = 5e-5) at 10Gbps NRZ, ER = 14 dB.

For the 25G APD, the sensitivity is -21 dBm (BER = 1e-12) and -27 dBm (BER = 5e-5) at 25Gbps NRZ, ER = 14 dB.

The insets of Fig. 4a-b show the measured bandwidth for bare APD chips at operating reverse bias voltage  $V_R = 90\% V_{BR}$ . The bandwidth remains stable up to an overload condition of  $P_{IN} = -3 \text{ dBm}$ .

### Conclusions

We demonstrated an optimized APD mesa structure which improves the optical damage threshold of the device, enabling safe operation up to +6 dBm and +10 dBm received optical input power for 25G and 10G APD, respectively. To the best of our knowledge, no APD of comparable speed was reported capable of operating without damage up to such high input power.

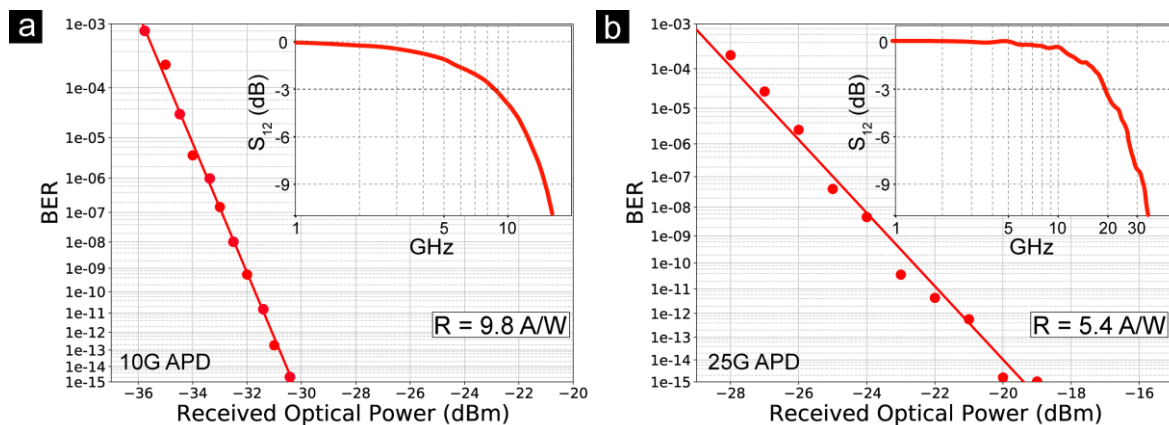


**Fig. 4:** APD ROSA sensitivity at  $\lambda = 1550 \text{ nm}$  for (a) 10G APD at 10 Gbps and (b) 25G APD at 25 Gbps. The insets show the frequency response at 90%  $V_{BR}$ . Measurements performed at  $T = 25 \text{ }^\circ\text{C}$ , NRZ PRBS  $2^{31}-1$  signal generator, ER = 14 dB.

## References

- [1] P. J. Winzer, "Scaling optical fiber networks: Challenges and solutions.", *Optics and Photonics News* 26.3, 28-35 (2015), DOI: [10.1364/OPN.26.3.000028](https://doi.org/10.1364/OPN.26.3.000028)
- [2] World Bank 2021, "World Development Report 2021: Data for Better Lives", Washington DC: World Bank (2021), DOI: [10.1596/978-1-4648-1600-0](https://doi.org/10.1596/978-1-4648-1600-0)
- [3] J. C. Campbell, "Advances in photodetectors," in *Optical Fiber Telecommunications, Vol. 5, Part A: Components and Subsystems*, 5th ed., edited by I. Kaminow, T. Li, and A. E. Wilner (Academic Press, 2008), ISBN: 978-0-240-81121-5
- [4] Technical Specifications 100G Lambda MSA, [Specifications \(100glambda.com\)](https://www.100gmsa.com/specifications)
- [5] J. J. S. Huang, H. S. Chang, and Y. H. Jan, "Reliability Scaling of Nanoscale Avalanche Photodiodes in High-Speed Optical Communication.", *Applied Physics Research* 11.6 (2019), DOI: [10.5539/apr.v11n6p1](https://doi.org/10.5539/apr.v11n6p1)
- [6] A. Ciarrocchi, W. Quan, M. Blaser, M. Hämmerli, and H. Meier, "Optical Damage Threshold Screening Methodology for 28 GBd, Long Wavelength Avalanche Photodiodes," in *Optical Fiber Communication Conference (OFC) 2022, Technical Digest Series* (Optica Publishing Group, 2022), paper Th2A.39, DOI: [10.1364/OFC.2022.Th2A.39](https://doi.org/10.1364/OFC.2022.Th2A.39)